JOURNAL OF APPLIED ELECTROCHEMISTRY 19 (1989) 720–728

Modelling of gas-evolving electrolysis cells. III. The *iR* drop at gas-evolving electrodes*

M. KUHN‡, G. KREYSA§

Dechema-Institut, Theodor-Heuss-Allee 25, D-6000 Frankfurt am Main 97, FRG

Received 15 August 1988; revised 2 February 1989

Based on a potentiostatic interrupter technique the *iR* drop of the bubble layer in front of gas-evolving electrodes of various shapes has been investigated. At small plane electrodes the dependency of *iR* drop on electrode inclination has been studied for hydrogen, oxygen and chlorine evolution. In all systems a slightly up-faced orientation results in a gas bubble layer structure of minimum *iR* drop. Also for expanded metal electrodes of different shapes the *iR* drop across the electrode diaphragm gap has been studied. The fractional open cross-section and the inclination angle of the electrode blades have been identified as important parameters with respect to the gas diverting effect. These tendencies have also been confirmed for a pilot cell of 1 m height.

Nomenclature

b' Tafel slope (V)
c_0 double layer capacity ($F\,cm^{-2}$)
d thickness (cm)
E electrode potential (V)
F Faraday number ($96487\,As\,mol^{-1}$)
i current density ($A\,cm^{-2}$)
R area resistance ($\Omega\,cm^2$)
R gas constant ($8.3144\,Ws\,deg^{-1}\,mol^{-1}$)
T temperature (K)
t time (s)
u_g^0 superficial gas velocity ($cm\,s^{-1}$)
u_{sw} swarm velocity ($cm\,s^{-1}$)
U voltage (V)

Greek symbols

α inclination angle (°)
β symmetry factor (1)
ε_g gas voidage (1)
ε_m maximum gas voidage (1)
η overvoltage (V)
κ electrolyte conductivity ($S\,cm^{-1}$)
ν_e number of electrons (1)

1. Introduction

In Parts I and II of this communication [1, 2] properties of electrogenerated bubble flow were treated. Part I presented a new model describing the gas voidage considering hindered bubble coalescence in the electrolyte. The introduction of the coalescence barrier model with its prediction of a limiting gas voidage, ε_m, for each gas/electrolyte combination resulted in a close agreement with experimental investigations.

In Part II the flow field structure in front of gas-evolving electrodes was investigated by means of the LDA technique [2]. The velocity component parallel to the electrode surface is much greater than expected from the literature [3]. Its value decreases sharply with increasing distance from the electrode. This velocity gradient causes a force due to static pressure drop directed towards the electrode surface, which explains the observation of a thin gas-loaded layer in the immediate vicinity of the electrode surface. It has been shown that the shape of the flow field at a gas-evolving electrode and the velocities therein are strongly affected by the hydrodynamic properties of the flow channel and the geometry of the electrode.

The purpose of this part is the correlation of bubble flow hydrodynamics, electrode and cell geometry with *iR* drop. The *iR* drop of the gas-loaded electrolyte is an important factor in practical electrolysis processes with gas evolution. The electrolyte resistivity is strongly dependent on gas voidage in the bubble flow and therefore this flow is an important factor for production costs with respect to the specific energy consumption.

There are a number of papers dealing with the effects of gas bubbles on electrolyte resistivity and cell voltage [4–7]. However, there is a lack of knowledge concerning the relation between electrode geometry and bubble flow around it. The bubble flow in the electrode gap and its properties, such as maximum gas voidage, ε_m, have to be investigated with respect to the influence of electrode and flow channel geometry and their consequences such as the resistivity of the gas-loaded electrolyte.

* Paper presented at the 2nd International Symposium on Electrolytic Bubbles organized jointly by the Electrochemical Technology Group of the Society of Chemical Industry and the Electrochemistry Group of the Royal Society of Chemistry and held at Imperial College, London, 31st May and 1st June 1988.

‡ *Present address*: Digital Equipment GmbH, Hahnstraße 25, D-6000 Frankfurt am Main, FRG.
§ Author to whom correspondence should be addressed.

0021-891X/89 $03.00 + .12

2. Computer-controlled electrochemical measurements with elimination of *iR* drop

A reliable method for determination of *iR* drop is a prerequisite for the experimental investigations. The potential measured between working and reference electrode is substantially influenced by *iR* drop if high current densities are applied or solutions with poor conductivity are used. The measured quantity is the sum of the true potential, *E*, and the ohmic drop.

$$E' = E + iR \tag{1}$$

Different methods are available for determination of *iR* drop. There are procedures with variation of distances between working electrode and Luggin capillary, impedance measurements and interrupter techniques [8, 9]. The method applied here is based on current interruption combined with computer control and data evaluation of the potential transients measured during interruption [10].

If experimental potential transients are available, a suitable extrapolation method is required for determination of the *iR*-free electrode potential. The schematic transient in Fig. 1 illustrates the problems involved in this *iR* determination technique. During the first few microseconds the potential transient is disturbed by interactions between electronic switch, electrolysis cell, potentiostat, and the wiring of the measured system. Potential measurement at any discrete time after interruption yields too low a potential and a too large *iR* drop. This means potential measurement at any discrete time results in an overcompensation of the polarization curve [11]. To avoid this error the whole potential transient has to be sampled to get the true *iR* drop by extrapolation to zero time. This extrapolation can be based on the Frumkin equation (Equation 2), which describes the time dependency of the electrode potential.

$$\eta(t) = \eta(0) - b' \ln\left(1 + \frac{i(0)}{b'C_0}\, t\right) \tag{2}$$

with

$$b' = \frac{RT}{\beta v_e F}$$

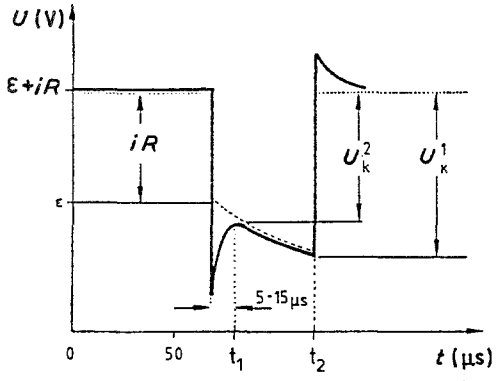

U_k^1, *IR drop measured with interrupter*

U_k^2, *IR drop measured with interrupter applying an optimum interrupter time*

Fig. 1. Potential transient with *iR* components.

The interrupter was designed for minimal disturbance and very fast response to the system under test. Precautions were taken for supressing the interactions of the standard electrochemical measuring equipment (e.g. potentiostat) with the cell while interrupting the current. The interrupter unit with its typical performance data is shown in Fig. 2.

With this unit, current flow through the cell is interrupted for a period of about 50 µs. During this time the transient is registered by a fast transient recorder (VUKO VKS 22-16, 8 bit resolution, 2 MHz sampling rate). The evaluation of transient data was made by means of a simplifed, logarithmic form of the Frumkin equation [10]

$$\ln \eta(t) = \ln \eta(0) - \frac{i(0)}{\eta(0)C_0}\, t \tag{3}$$

By means of this relation the potential can be approximately treated as a linear function of time. Figure 3 shows an application example for this method. Cathodic polarization curves for hydrogen evolution at platinum in 2.8 M sulphuric acid are given with and without *iR* elimination. Due to the large *iR* drop the uncorrected curve (1) in Fig. 3 is almost a straight line. The corrected data (2), without *iR* drop, result in a straight line with a Tafel slope of 27 mV (Fig. 4). This example with its reasonable result for the Tafel slope at current densities up to 1 A cm^{-2} demonstrates the reliability of the method [12].

3. *iR* drop at inclined electrodes

Expanded metal electrodes, which are used in many industrial electrolyzers, consists predominantly of small inclined electrode planes, the inclination angle being dependent on the degree of expansion. Therefore, the *iR* drop in front of small inclined model electrodes has been studied. This *iR* drop depends on the gas voidage and the velocity of the bubble flow and the thickness of the gas bubble layer. These quantities are influenced by: (1) the maximum gas voidage, ε_m, which causes a certain thickness of the gas loaded layer; (2) the buoyancy, which drives the flow of the layer and yields a decompression at up-faced and a compression at down-faced electrode inclinations, respectively; (3) the compression force based on the velocity gradient perpendicular to the electrode surface described by Bernoulli's law [2].

The coalescence barrier model with the maximum gas voidage was used for a theoretical prediction of the dependency of *iR* drop on thickness of the gas-loaded layer. The model system consisted of an electrode chamber with the dimensions 1 cm height, 1 cm depth and 10 cm width, e.g. distance between the electrodes. A constant volumetric gas flow rate was supplied to this chamber while varying the width of the gas-loaded cross-section from 0 to 10 cm. By use of Equation 4, which is derived from the assumption of zero liquid flow [1], the gas voidage, ε_g, can be

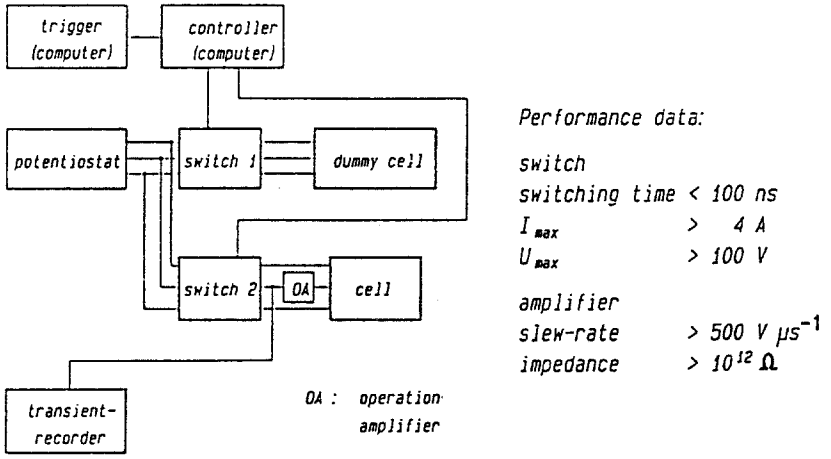

Fig. 2. Interrupter unit with performance data.

calculated from the known superficial gas velocity, u_g^0.

$$\varepsilon_g = \frac{\varepsilon_m}{\left(1 + \frac{\varepsilon_m u_{sw}}{u_g^0}\right)} \quad (4)$$

with ε_m the maximum gas voidage of the gas/electrolyte combination under examination and u_{sw} the bubble swarm velocity, determined by the Marrucci equation [13]. By means of the Maxwell–Nader equation for the determination of the gas/liquid mixture resistivity [14, 15] and the width of the gas-loaded layer a normalized cell resistance was obtained by Equation 5.

$$\frac{R}{R_0} = \frac{R_{\text{gas-loaded layer}} + R_{\text{gas-free layer}}}{R_{\text{gas-free cell}}} \quad (5)$$

Figure 5 shows the dependency of the normalized cell resistance on width of the gas-loaded layer. This example is based on the following figures: hydrogen evolution in 20% KOH, maximum gas voidage $\varepsilon_m = 0.27$ [1], volumetric gas flow rate 2 $cm^3 s^{-1}$.

Figure 5 shows a dependency, which can be divided into two parts separated by a maximum of cell resistance. At small widths of the gas-loaded layer the gas voidage is at its maximum. Under the condition of constant gas voidage and, therefore, solution resistivity an expansion of the layer causes a linear increase in resistance. If the expansion of the gas layer exceeds a certain thickness the gas voidage decreases due to the decreased superficial gas velocity. In this part the normalized cell resistance declines with further expansion of the gas-loaded layer.

The experimental investigation of the dependency of the *iR* drop on electrode inclination angle is aimed towards the verification of these predictions and the applicability of the coalescence barrier model. Recommendations for optimum inclination angles of electrodes should also be obtained.

3.1. *Experimental details*

Planar electrodes were chosen as a model system. The 1 × 1 cm flat plate electrodes were fixed in an acrylate support. Non-uniform current distributions based on bubble accumulation were diminished by the small electrode dimensions [7]. In order to avoid changes in potential and current distribution with variation of inclination angle of the working electrode, both electrodes were mounted on a pivoted disc in a fixed parallel position. Therefore changes in inclination did not change the relative position between the electrodes. The Luggin probe was mounted in a fixed position at a distance of 8 mm from the working electrode. This distance was always larger than the thickness of the gas-loaded layer. The electrolysis cell was controlled potentiostatically (Wenking ST72) and equipped with the aforementioned computer-

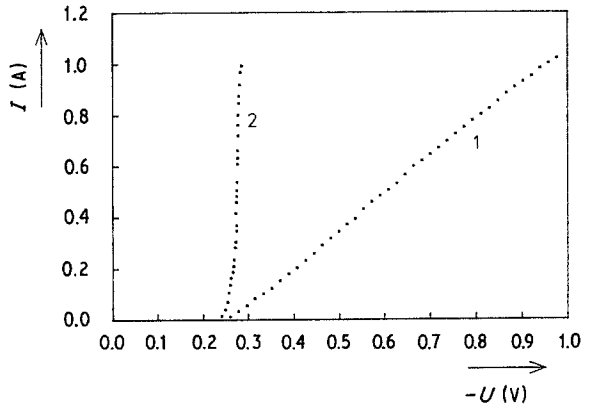

Fig. 3. Polarization curve for hydrogen evolution at flat plate platinum electrode, 2.8 M H_2SO_4. (1) Without, (2) with *iR* drop elimination.

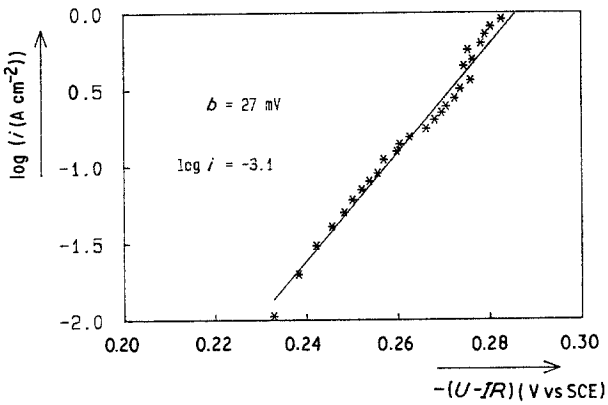

Fig. 4. Tafel plot with *iR* drop elimination for hydrogen evolution at flat plate platinum, 2.8 M H_2SO_4.

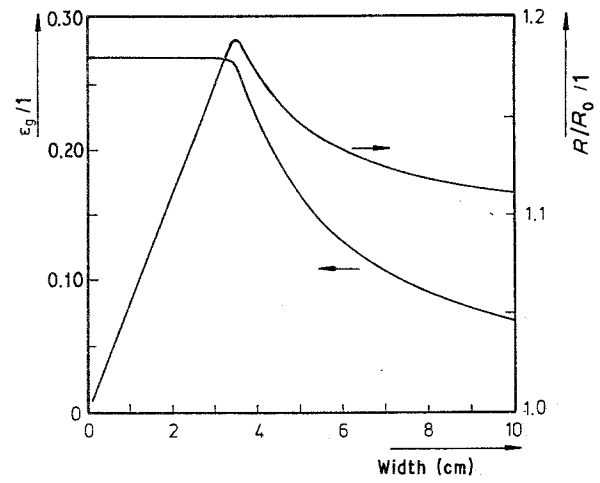

Fig. 5. Gas voidage and normalized cell resistance as function of the thickness of the gas loaded electrolyte layer.

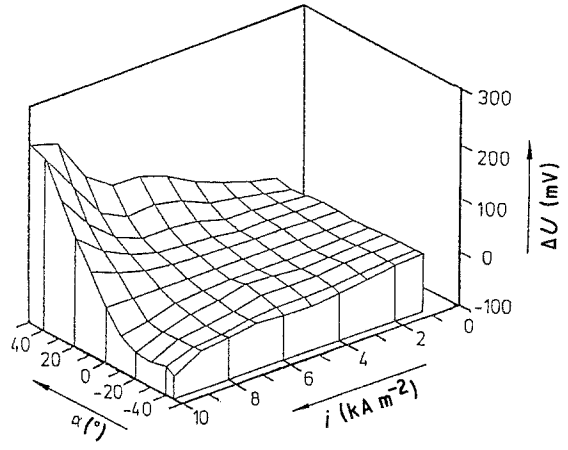

Fig. 7. *iR* drop variation as function of current density and inclination angle variation for chlorine evolution; activated titanium electrode, 5.08 M NaCl + 2.0 M HCl.

controlled measurement system for determination of *iR* drop. Measurements were carried out over a range of inclination angles from $-45°$ (up-faced) to 50° (down-faced) and current densities between 0.1 and 1.0 A cm^{-2}. Comparable results for *iR* drop at different current densities were obtained by applying the normalization

$$\Delta U = iR(\alpha) - iR(0) \quad (6)$$

where $iR(0)$ is the *iR* drop measured at a vertical electrode. The ΔU value in Equation 6 represents the part of the overall *iR* drop, which is mainly determined by variation of inclination angle.

3.2. *Results and discussion*

Table I gives the tested systems with an estimation of the optimum inclination angle, if there is a minimun in the *iR* drop/inclination angle dependency.

There are three distinct groups of results which are represented by Figs 6, 7 and 8. Fig. 6 shows the behaviour of hydrogen evolution in alkaline solution. A decrease in *iR* drop with increased expansion of the gas-loaded layer is observed. Chlorine (Fig. 7) and oxygen evolution show a decrease with expansion of the bubble layer but after exceeding a minimum *iR* drop between -10 to $-30°$ inclination a moderate increase in ohmic drop can be observed. Hydrogen evolution in sulphuric acid (Fig. 8) shows, in parts, a similar behaviour but at about 20° down-faced inclination there is a maximum in *iR* drop. Further compression of the gas bubble layer results in a decrease of ohmic drop. This corresponds very well with the expected behaviour discussed above if the gas voidage reaches its limiting value. The small maximum gas voidage ($\varepsilon_m = 0.13$) of the system hydrogen/sulphuric acid, which is the smallest one of all investigated combinations, gives further support to this explanation. All other systems do not reach the region of maximum gas voidage in bubble flow due to higher limiting voidages. These systems are located on the right side from the maximum in the cell resistance curve of Fig. 5. An expansion of the gas-loaded layer leads to a reduction of *iR* drop. The optimum inclination angles for minimum *iR* drop are also given in Table 1. For certain gas/electrolyte combinations an increase of ohmic drop is observed for strong gas layer expansions. This may be explained by a decrease of bubble layer flow velocity which is accompanied by a larger number of bubbles adhering to the electrode and shielding a part of the electrode which results in an increase of *iR* drop under these circumstances.

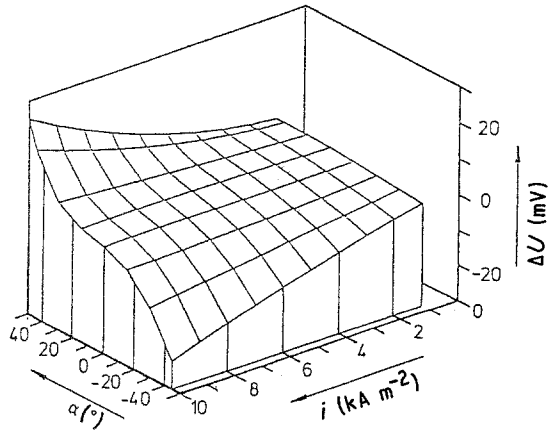

Fig. 6. *iR* drop variation as function of current density and inclination angle variation for hydrogen evolution; platinum electrode, 4.0 M NaOH.

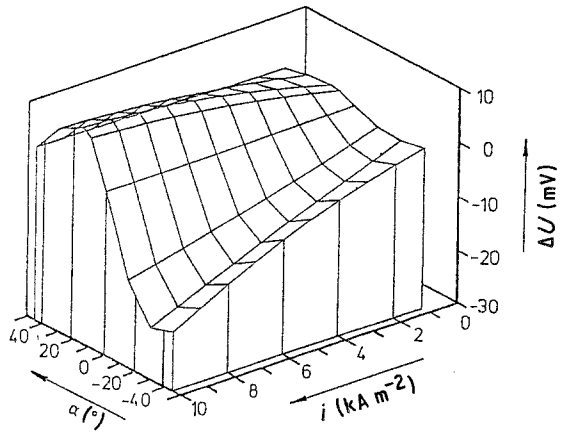

Fig. 8. *iR* drop variation as function of current density and inclination angle variation for hydrogen evolution; platinum electrode, 1.68 M H_2SO_4.

Table 1. Electrochemical systems for determination of iR drop dependency on electrode inclination angle

Electrode	*Product*	*Electrolyte*	*Recommended inclination angle*
DSA	Chlorine	25.0% (5.08 M) NaCl + 2.00 M HCl	−30°
Platinum	Hydrogen	15.0% (1.68 M) H_2SO_4	−30°
Nickel	Oxygen	30.0% (6.85 M) KOH	−15°
Platinum	Hydrogen	13.9% (4.00 M) NaOH	-
Platinum	Hydrogen	19.1% (4.00 M) KOH	-
Nickel	Hydrogen	30.0% (6.85 M) KOH	-

The results give evidence for the impact of the limiting gas voidage, ε_m, on *iR* drop. An effect of electrode material on ohmic drop could not be deduced from these investigations.

4. *iR* drop at expanded metal electrodes

At small inclined electrodes it has been shown that the *iR* drop is affected by the maximum gas voidage of the gas/electrolyte combination and geometrical factors of the electrode (e.g. inclination angle). Therefore a correlation between these two groups of influences and *iR* drop should also be obtained for a more complex electrode geometry.

4.1. *Geometrical quantities of expanded metals*

In contrast to the single parameter of inclination angle at flat plate electrodes the structure of an expanded metal needs further geometrical quantities for full description. Figure 9 shows a front and a side view of expanded metal.

Only some of the quantities given in Fig. 9 can directly be taken from the manufacturer's description or by direct measurement (Table 2). Further deduced quantities which may influence the electrochemical reaction or the bubble flow around the electrode and which could be a measure for electrode performance with respect to *iR* drop are listed in Table 3.

For the investigation of the impact of expanded metal structure on *iR* drop, a set of different geometries has been selected. Table 4 collects the typical quantities for these selected structures.

4.2. *Experimental details*

The investigations were carried out in a small circular membrane cell. An inner diameter of 6.8 cm for the cell corresponds to a diameter of 6.6 cm for the electrodes. The electrode compartment was 1.7 cm in depth and the electrode/membrane gap was about 0.1 cm. 30% KOH solution was used in both electrode compartments with a flow rate of about 100 $cm^3 h^{-1}$ each. The Luggin probe was positioned from the rear through holes in the

Table 2. Known and measured expanded metal quantities

l length of mesh	manufacturer's details
b width of mesh	
c half width of bridge	
u strand width	
s thickness of metal	
a effective thickness of expanded metal	measured quantity

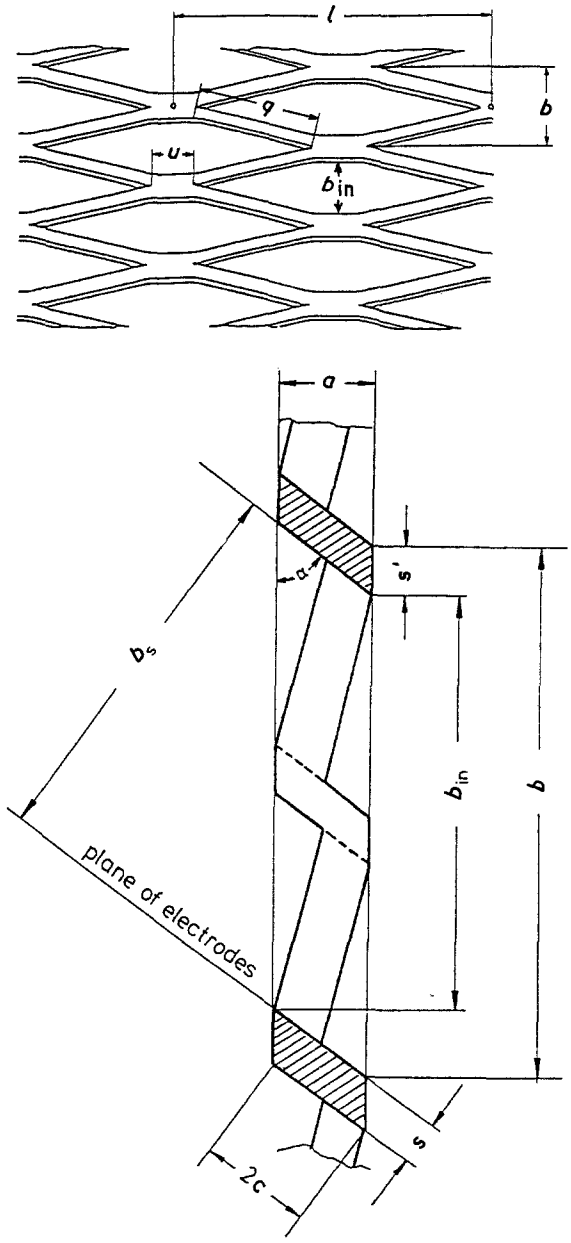

Fig. 9. Front and side view of expanded metal.

Table 3. Calculated quantities of expanded metals

α inclination angle

$$\alpha = \arcsin\left(\frac{a}{2c}\right)$$

b_2 inner width of mesh perpendicular to the plane of electrodes

$$b_s = b \sin(\alpha) - s$$

f_{real} total electrode surface related to electrode current cross-section

$$f_{real} = \frac{4[2c(u + q) + s(u + 2q)]}{bl}$$

with $b_{in} = b_s \sin(\alpha)$

$$q' = \tfrac{1}{2}\sqrt{b_{in}^2 + (1 - 2u)^2}$$

$$q = \sqrt{\frac{a^2}{4} + q'^2}$$ length of traverse bridge

f_c projected close electrode area related to the current cross-section

$$f_c = \frac{2[2c'(u + q') + s'u + 2s''q']}{bl}$$

with $c' = c \cos(\alpha)$

$s' = s/\sin(\alpha)$

$s'' = s \sin(\alpha)$

f_p open area of the electrode projected to the plane perpendicular to the plane of electrodes related to electrode area in the plane

$$f_p = 1 - \frac{2s(u + 2q')}{(b_s + s)l}$$

expanded metal in front of the electrode plane. The selected expanded metals were used anodically and cathodically for water electrolysis. A conditioning pre-electrolysis was performed before each measurement for about 2 h with a current of 3 A. iR drop determination was based on the aforementioned computer-controlled measuring system. Current was varied from 1 to 10 A, corresponding to 0.3–3 kA m^{-2} of current density.

Table 4. Typical quantities for selected expanded metal structures

Expanded metal	016/2010	163/2510	168/1510	168/2010	285/2010
a (mm)	3.1	2.4	2.4	3.0	3.3
l (mm)	16	16	16	16	28
b (mm)	7	6	8	8	6
c (mm)	2	2.5	1.5	2	2
s (mm)	1	1	1	1	1
u (mm)	2	5.6	2.1	2.1	10.6
α (grd)	50.8	28.7	53.1	48.6	55.6
b_s (mm)	4.42	1.88	5.40	5.00	3.95
f_{real}/l	1.73	2.19	1.26	1.52	1.85
f_c/l	0.59	1.03	0.43	0.53	0.61
f_p/l	0.67	0.54	0.71	0.70	0.74

4.3. *Results and discussion*

It has been shown [16] that the difference, ΔU, between iR drop with gas-loaded electrode/membrane gap, iR_{gas}, and the ohmic drop without gas, $iR_{gas\,free}$ (Equation 7)

$$\Delta U = iR_{gas} - iR_{gas\,free} \quad (7)$$

can be determined by neglecting the gas bubble influence on iR drop at low current densities ($\leqslant 0.3$ kA m^{-2}). This voltage difference is proportional the gas voidage of electrolyte in the gap

$$\Delta U \sim \varepsilon_g i \quad (8)$$

An empirical equation based on Equation 8 was used for evaluation of the measured data [16]

$$\Delta U = a + mi \quad \text{with } m \approx \frac{2d\varepsilon_g}{\kappa} \quad (9)$$

The slope of the straight line (m) is a measure of gas voidage and, therefore, the resistivity of the bubble layer at the electrode. The approximate expression for m in Equation 9 was derived by an estimation of the resistance of the gas-loaded layer of the thickness d, not taking into account that ε_g itself is a function of i [16]. Therefore a strong linearity between ΔU and i can only be expected at high currents if the gas voidage approaches its limiting value, ε_m. The parameter m should be a function of the geometrical quantities of the expanded metals and of the limiting gas voidage, ε_m, for the gas/electrolyte combination. Figures 10 and 11 show a relative iR drop increase with increasing current density for oxygen and hydrogen evolution.

For the iR drop difference data above 6 A cell current the slopes of the straight lines which are shown in Figs 10 and 11 were determined. Table 5 gives these parameters. These experimental slopes correspond to the slope m in Equation 9. A regression analysis was undertaken with these data for determination of relevant geometrical factors for the description of iR drop. Several empirical correlations were tested and selected by means of the minimum standard deviation.

The determined equation for oxygen evolution describing expanded metal performance with respect to iR drop as a function of geometric quantities is

$$m \times 10^3 = a_1 + a_2 f_{real} + a_3 f_p + a_4 f_{real} f_p \quad (10)$$

Table 5. Slopes of the straight iR drop difference/current dependency for hydrogen and oxygen evolution at various expanded metal structures

Expanded metal	Slope (oxygen) (ohm cm^2)	Slope (hydrogen) (ohm cm^2)
016/2010	5.15×10^{-3}	10.82×10^{-3}
163/2510	2.62×10^{-3}	9.97×10^{-3}
168/1510	7.01×10^{-3}	6.70×10^{-3}
168/2010	7.20×10^{-3}	6.27×10^{-3}
285/2010	8.36×10^{-3}	9.22×10^{-3}

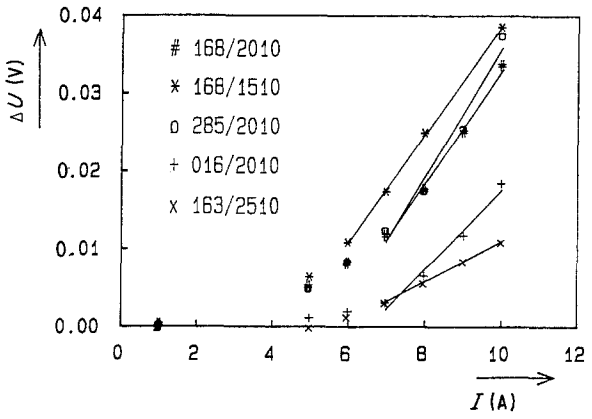

Fig. 10. *iR* drop differences as function of current for oxygen evolution; nickel electrodes, 30% KOH.

with

$$a_1 = -75.95$$
$$a_2 = 29.25$$
$$a_3 = 117.33$$
$$a_4 = -41.32$$

The maximum deviation between calculated and experimental m values is 7.3%

Figure 12 shows a decline in m and better performance with decreasing total surface (f_{real}) and decreasing transparancy (f_p) of the electrode. A decrease in f_{real} corresponds to an increase in local current density. The transparency, f_p, of the electrode influences the flow through the expanded metal from front to rear side transporting the gas behind the electrode.

The performance of expanded metal electrodes for hydrogen evolution is described by Equation 11.

$$m \times 10^3 = a_1 + a_2 f_{real} + a_3 f_p + a_4 \frac{f_{real}}{f_p} \qquad (11)$$

with

$$a_1 = 64.05$$
$$a_2 = 32.88$$
$$a_3 = -93.78$$
$$a_4 = -18.59$$

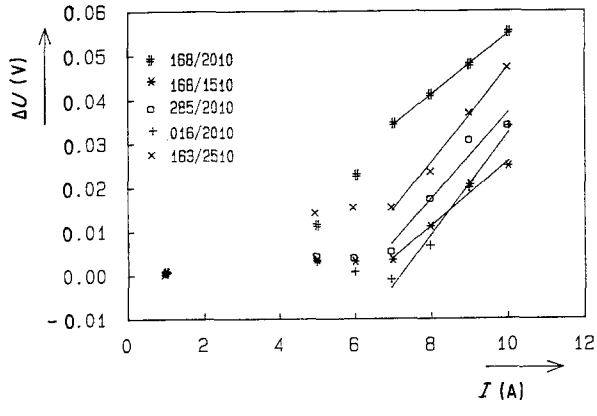

Fig. 11. *iR* drop differences as function of current for hydrogen evolution; nickel electrodes, 30% KOH.

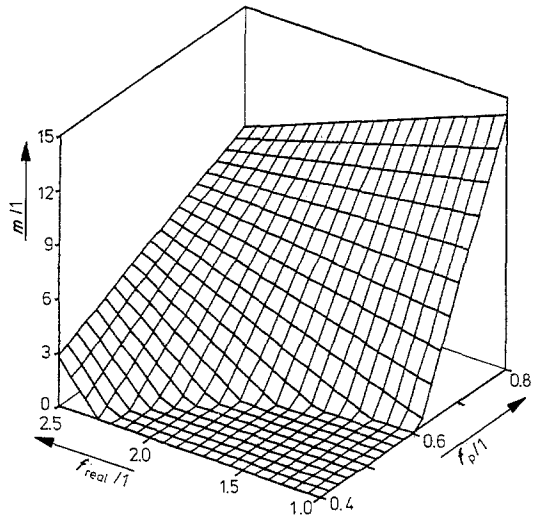

Fig. 12. Performance parameter b of expanded metal as function of f_{real} and f_p according to Equation 10 for oxygen evolution.

The maximum deviation between calculated and experimental m values is 28%. The relatively large errors are due to the fact that only 5 points were available to determine 4 coefficients.

Figure 13 shows a decline in m with smaller value of the total electrode surface (f_{real}). The influence of the transparency shows a maximum of m moving with higher f_{real} values towards higher f_p values. But also in this case m decrease mainly with decreasing f_p. This means that a smaller transparency, f_p, forces the flow towards the rear of the electrode. In the case of large transparency more gas can rise in front of the electrode. By comparison of Figs. 12 and 13 it becomes obvious that the same parameters are influencing the performance of an oxygen- and hydrogen-evolving electrode in a differnt manner. Equations 10 and 11 also show by the a_4 terms that different gas/electrolyte combinations possess different performance equations.

5. Investigations at a larger vertical cell

For verification of the above relationships between geometrical quantities and *iR* drop, which are based

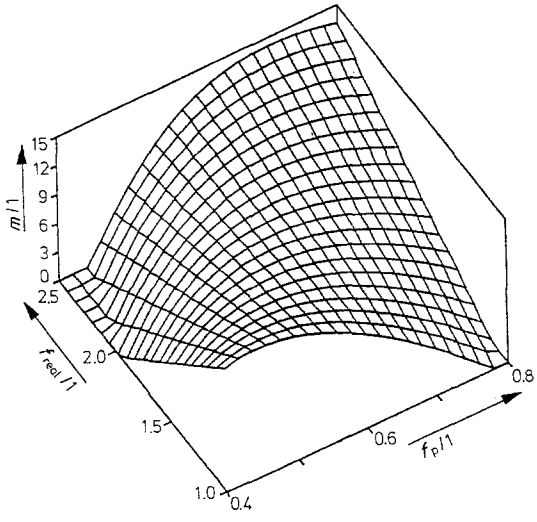

Fig. 13. Performance parameter b of expanded metal as function of f_{real} and f_p according to Equation 11 for hydrogen evolution.

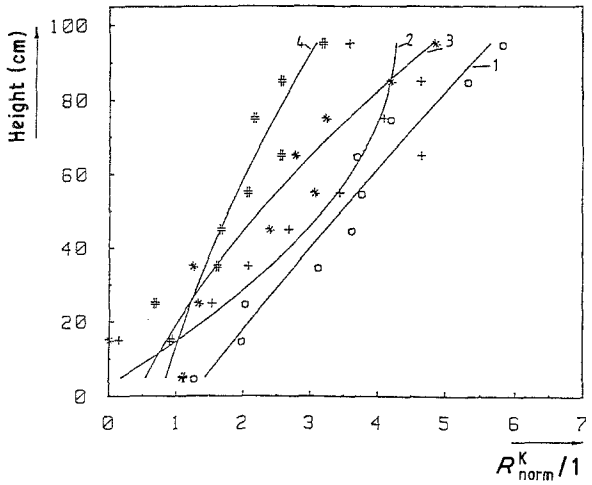

Fig. 14. Normalized resistance over electrode gap; hydrogen evolution, 26% NaOH, different electrode geometries: flat plate (slope 1), expanded metal type 163/2510 (slope 2), type 168/2010 (slope 3), type 168/2010 with flow separator (slope 4).

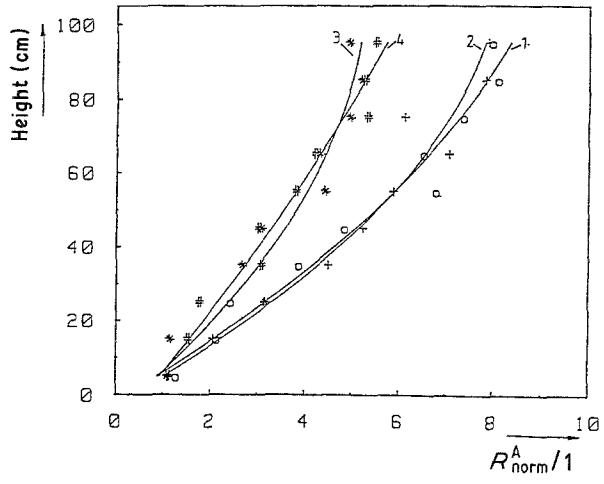

Fig. 15. Normalized resistance over electrode gap; oxygen evolution, 26% NaOH, different electrode geometries: flat plate (slope 1), expanded metal type 168/2010 (slope 2), type 163/2510 (slope 3), type 163/2510 with flow separator (slope 4).

on measurements in a small membrane cell, tests in a larger vertical membrane cell were conducted.

5.1. *Experimental details*

The experiments were carried out in a cell consisting of two acrylate electrode compartments and an acrylate middle compartment, which was used for potential measurements. All parts were reinforced with steel frames. The electrode compartments had inner dimensions of 103.4 cm height, 5.2 cm width and 3.0 cm depth; the middle compartment was 9.0 cm in thickness. The electrodes were 100 cm in height and 5.0 cm in width. Thermocouples were positioned from the top of the electrode compartments at heights between 5.0 and 95.0 cm. The same holds for the two Luggin probes, which were positioned in the middle compartment. Two membrances (Nafion Type 901) were used as separators. All measurements were taken with 60 l electrolyte solution (26% NaOH), a current of 250 A, corresponding to a current density of 5 kA m^{-2}. Stability of temperature was guaranteed by means of a cryostat. Potential and temperature distribution was measured every 10 cm from 5 to 95 cm height of cell.

5.2. *Results and discussion*

The relevant quantity, the *iR* drop between electrode and membrane was determined on the basis of an analysis of cell potential [17]. Due to a temperature increase with height of cell, the resulting data must be corrected for temperature dependence and have been related to a temperature of 25° C [16]. These values normalized to the resistance of the gas-free electrode gap at 25° C are shown in Figs 14 and 15 for hydrogen and oxygen evolution, respectively.

While performance factor b (Equation 9) is a measure of gas voidage and describes the ability of a certain expanded metal structure to divert the gas bubble flow, the curves in Figs. 14 and 15 can be treated in a similar way. Their slope-normalized resistivity, which is proportional to gas voidage, versus height of cell, is also a description of the properties of an expanded metal with respect to diverting the bubble flow. These two quantities are useful as a basis of a qualitative comparison. A similarity in their trends would support the assumption that the correlations for expanded metal performance (Equations 10–12) found in the small membrane cell also can be applied to systems of larger scale.

A rough estimation of the slope b' of the straight lines made up by the normalized resistivity as a function of electrode height yields the results in Table 6, which compares the performance parameters (e.g. slopes) b and b' for the small and the large cell.

The data from different cell sizes in Table 6 agree well in trend and facilitate an optimization of electrode geometry for alkaline water electrolysis based on Equation 10 and 11.

Table 6. Comparison of performance parameters of different expanded metal structures at different cell sizes

Expanded metal	H_2 evolution Cell size		O_2 evolution Cell size	
	Small (ohm cm^{-1})	Large	Small (ohm cm^{-1})	Large
163/2510	9.97×10^{-3}	4.02×10^{-2}	2.62×10^{-3}	4.75×10^{-2}
168/2010	6.27×10^{-3}	3.26×10^{-2}	7.20×10^{-3}	8.17×10^{-3}

6. Conclusions

For small planar electrodes it has been found that the inclination angle strongly influences the *iR* drop of the bubble curtain in front of these electrodes. In general, with increasing up-faced orientation of the electrode the *iR* drop decreases. In some cases a minimum *iR* drop at slightly up-faced oriented electrodes could be observed. For hydrogen evolution in acid solution a maximum *iR* drop was found for a certain down-faced orientation of the electrode.

This behaviour can be explained qualitatively by the coalescence barrier model [1]. For expanded metal sheet electrodes the influence of different geometrical parameters on the *iR* drop across the electrode diaphragm gap was studied in a laboratory cell. It was found that the inclination angle of the electrode blades and the open fraction of the electrode area (transparency) are parameters of great importance. Empirical correlations were obtained which are useful for geometrical electrode optimization. Furthermore, it was shown that expanded metal electrodes of different geometry possess, in a 1 m high cell, broadly the same behaviour as that observed in a smaller laboratory cell. This means that test experiments for the comparison of different expanded metal electrodes in a laboratory cell allow a prediction of their behaviour in industrial cells.

Acknowledgement

The authors would like to acknowledge financial support of this work by Arbeitsgemeinschaft Industrieller Forschungsvereinigungen (AIF).

References

[1] G. Kreysa and M. Kuhn, *J. Appl. Electrochem.* **15** (1985) 517.
[2] G. Kreysa and M. Kuhn, *J. Appl. Electrochem.* submitted.
[3] B. E. Bongennaar-Schlenter, Thesis, TH Eindhoven (1984).
[4] O. Lanzi and R. F. Savinell, *J. Electrochem. Soc.* **130** (1983) 799.
[5] D. A. G. Bruggemann, *Ann. Phys.* **24** (1935) 636.
[6] C. W. Tobias, *J. Electrochem. Soc.* **106** (1959) 833.
[7] G. Kreysa and H.-J. Külps, *J. Electrochem. Soc.* **128** (1981) 979.
[8] D. Britz, *J. Electroanal. Chem.* **88** (1978) 309.
[9] M. Hayes and A. T. Kuhn, *J. Power Sources* **2** (1977/78) 121.
[10] M. Kuhn, G. Kreysa and B. Hakansson, Proc. 34th ISE-Meeting, Erlangen (1983).
[11] B. Elsener and H. Böhni, *WuK* **33** (1982) 207.
[12] M. Kuhn, K.-G. Schütze, G. Kreysa and E. Heitz, *Dechema Mono.* **101** (1986) 265.
[13] G. Marrucci, *Ind. Eng. Chem. Fund.* **4** (1965) 224.
[14] J. C. Maxwell, 'A Treatise on Electricity and Magnetism', 2nd edn. Vol. 1, Clarendon Press, Oxford (1881).
[15] G. H. Neale and W. K. Nadar, *AIChE J.* **19** (1973) 112.
[16] M. Kuhn, Thesis, Universität Dortmund (1988).
[17] E. Heitz and G. Kreysa, 'Principles of Electrochemical Engineering', VCH Verlagsgesellschaft, Weinheim (1986).